# Experimental Verification of CFD Modeling of Turbulent Flow over Circular Cavities using FLUENT

T Hering, J Dybenko, E Savory

*Mech. & Material Engineering Dept., University of Western Ontario, London, Ontario*

*thering@uwo.ca , jdybenko@uwo.ca , esavory@eng.uwo.ca*

The commercial finite-volume CFD code FLUENT (ver.6.2) was used to simulate turbulent flow over a circular cavity at a variety of cavity depths. The accuracy and validity of the CFD results were compared to experimental data collected in a wind tunnel for the same cavity configurations. First, the approaching flow was compared. This was necessary in order to account for the influence of boundary layer effects on the resulting cavity flow. Then, pressure distributions along the cavity surfaces, obtained from pressure transducer measurements and wake velocity profiles, gathered from hot-wire anemometry measurements served as a basis for comparison between the experimental and simulated results. For certain circular cavity configurations the resulting mean flow field has been experimentally observed to be asymmetric in nature. This asymmetry was also observed in the FLUENT simulations, although the asymmetry was not as strong as seen in the experimental results. For symmetric cavity flow the simulated results showed good agreement with the experimental results in terms of the major physics of the flow and the drag coefficient due to the cavity. In all the cases examined, FLUENT underestimated the pressures along the cavity surface. Future work will examine the effects of applying different turbulence models to the simulations in order to determine if the current model is superior to other models in simulating cavity flows. An unsteady solution will also be sought.

## 1. INTRODUCTION

Cavities are a special type of surface irregularity and can be thought of as holes of different geometry that may arise from manufacturing and assemble limitations. They are especially important in aerodynamic applications. Some examples include landing gear wheel wells and rivet depressions on aircraft wings. Examining the flow structure over and around cavities becomes important in understanding the resulting drag force on the entire surface due to the cavity.

In the current investigation cavities of circular planform area were simulated using the commercial finite-volume code FLUENT (version 6.2). The simulated results were then compared to experimental data conducted in a wind tunnel setup for cavities with varying depth configurations.

Previous research has led to the identification of a certain cavity depth to diameter ratio (approximately 0.5), where mean asymmetric flow is observed for a circular cavity. Therefore, the main purpose of the investigation is to determine if the software FLUENT can model asymmetric mean flow for a symmetric cavity. A comparison was also made for symmetric flow configurations at other cavity depth/diameter ratios of 0.2 and 0.7.

## 2. CIRCULAR CAVITY FLOW REGIMES

Cavity flows in general have been characterized into two distinct types, “open” and “closed”. The “open” case is where the shear layer spans the cavity [1]. A large stable vortex can be observed within most of these types of configurations. This usually occurs for deep cavities, where the cavity depth to span wise ratio is quite large, i.e. cavities where the depth is greater than 0.1 of the cavity width. Circular cavity configurations are usually represented in terms of their depth to diameter ratios (h/D). Cavity parameters and the coordinate system used are shown in Figure 1. The “closed’ case usually occurs in shallow cavities, where the

depth to width ratio is small. In these types of cavities the shear layer separates at the upstream edge and reattaches to the cavity base somewhere in the middle of the cavity. Then it separates from the base and reattaches to the downstream edge of the cavity, as seen in Figure 2.

This h/D ratio is one important variable when determining the type of resulting cavity flow. Previous research suggests an h/D ratio of 0.1 is the limiting value between open and closed rectangular cavities [1].

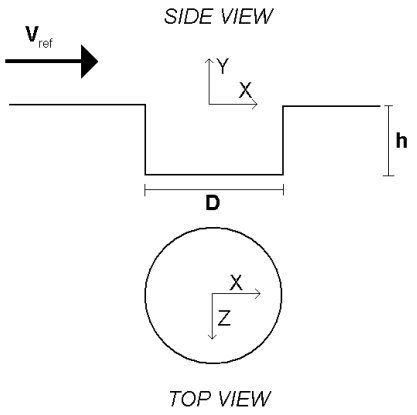


*Figure 1: Coordinate system and reference parameters used in the experiment and simulations*

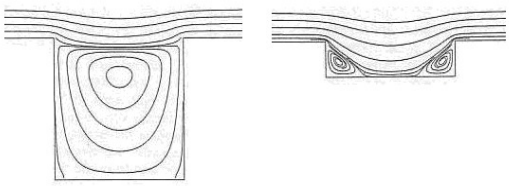

*Figure 2: Stream lines for different cavity types, "open"(left) and "closed" (right) [2]*

Circular cavities were first studied by Friesing [3], who noticed an asymmetric flow at certain h/D ratios. Other experimentalists such as [4, 5] have verified that this asymmetric flow occurs around h/D = 0.5. At these specific ratios the stable vortex found in open cavities is yawed with respect to the free stream direction. The vortex tube is yawed by approximately 45˚ to the free stream and it also protrudes out of the cavity as seen in Figure 3. Since the vortex tube extends beyond the cavity volume, the boundary layer flow above the cavity is affected more than for an open cavity. This results in the asymmetric flow and a larger drag force as first documented by [6].

This asymmetric flow has been documented as being marginally stable [4]. The asymmetry is capable of switching sense, across the stream wise axis, due to large disturbances in the flow.

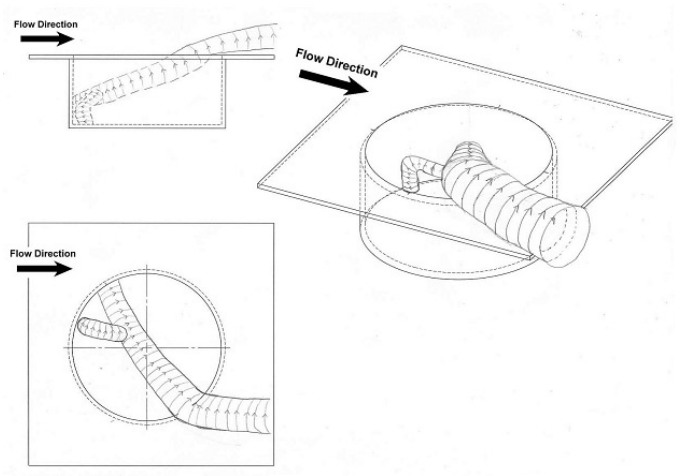


*Figure 3: Asymmetric vortex flow diagram [7]*

## 3. EXPERIMENTAL PROCEDURE AND PARAMETERS

The experiments were conducted in a closed loop wind tunnel in the Boundary Layer Wind Tunnel Laboratory at the University of Western Ontario. The cavity diameter was 76 mm and had a variable base in order to create different cavity height / diameter (h/D) configurations. The tunnel working section dimensions with regard to the cavity diameter were 2.8D (height) x 8D (width) x 85.5D (length). The cavity model was placed a distance of 56.5D downstream of the tunnel working section entrance. This was necessary in order for a thick boundary layer to develop. This location also provided steady boundary layer parameters, as the boundary layer thickness and skin friction coefficient across the span of the tunnel varied by +/- 9% and +/- 3%, respectively.

Using hot-wire anemometry the approaching flow was well documented. The free stream velocity was found to be 27 m/s and varied by 0.5 % across the span of the working section during the course of the experiments.

Once the approaching flow was well defined, hot wire anemometry measurements were made in the wake of the cavity for several configurations.

The 3 different cavity configurations tested were h/D = 0.2, 0.47 and 0.7, providing a wide range of flow fields. The h/D ratio of 0.47 was chosen due to its resulting asymmetric flow. After examining the cavity wake flows, pressure transducers were used to define a pressure distribution in terms of the pressure coefficient on the cavity surfaces and surrounding ground plane.

The pressure coefficient, Cp, is defined as:

$$Cp = \frac{P - P_s}{\frac{1}{2}\rho U_o^2} \qquad (1)$$

Where P is a measured pressure on a surface and $P_s$ is the static pressure measured in the free stream, ρ is the density of the working fluid and Uo is a reference velocity. The free stream velocity is most often used as the reference velocity, although normalizing the pressure coefficient using the friction velocity partially takes into account the influence of different boundary layers on the resulting pressure distributions.

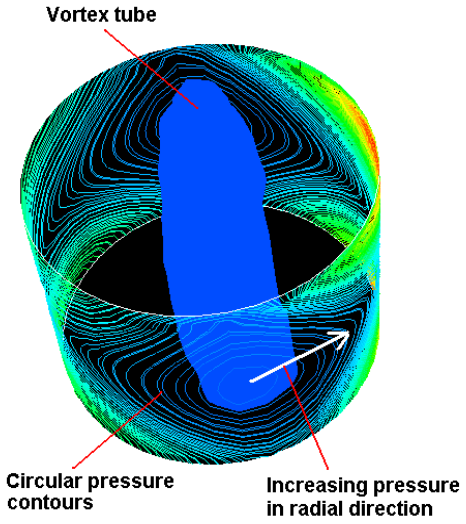


*Figure 4: Pressure contours on cavity sidewall showing the identification of a vortex tube*

Examining mean surface pressure contours can be used along with other data to identify flow fields and estimate shear layer separation and attachment locations. Regions of high mean Cp values can correspond to an impingement location. As mentioned by [8], a coherent vortex tube is sometime identifiable by looking for circular regions of low pressure surrounded by increasing pressure in the radial direction. In such a case when a vortex is involved the low pressure area corresponds to the centre of rotation of the vortex. An example of an identification of a vortex tube is shown in Figure 4. The vortex tube is shown with a constant low Cp value.

## 4. COMPUTATIONAL PROCEDURE AND SETUP

The following sections describe the process involved in setting up and creating the simulated results in the FLUENT software. Due to computational constraints and time, a steady state solution was sought. This resulted in only the mean experimental data being used in the comparison to the simulated data.

### 4.1 Computational Mesh

The main computational domain involved the modeling of a wind tunnel with the cavity cut into the floor of the working section, similar to the experimental tunnel. The wind tunnel was modeled in order to build up a similar boundary layer to that in the conducted experiments.

The simulated tunnel dimensions were normalized by the circular cavity diameter (D) and resulted in the tunnel having dimensions 4D (height) x 5.5D (width) x 47.3D (length). The width and height of the tunnel ensured that the boundary layers on the sides and top would not affect the flow field resulting from the cavity. Also the outlet conditions were placed far enough from the cavity to ensure no end effects would be observed around the cavity.

Due to the circular shape a structured grid was difficult to create. To get around this problem the wind tunnel model was divided into several smaller volumes that could individually be meshed with a structured grid. The tunnel base was meshed first, which was then projected along the tunnel height with varying grid points in order to capture the boundary layer profile above the ground plane. The grid spacing was kept constant inside the cavity located in the ground plane. This meant the smallest grid spacing was used inside the cavity just below the boundary layer mesh. Grid spacing was increased in areas far from the cavity in order to limit computation time.

## 4.2 Numerical Model and Parameters

The CFD model was simulated in FLUENT (ver 6.2) using a steady state 3D segregated implicit solver. Due to the shear layer separation at the leading edge of the cavity, a turbulence model capable of capturing shear layer separation was required. Hence the Reynolds Stress Model (RSM) was chosen [9].

For the Reynolds stress model the default model constants were used. Standard wall functions were applied for near wall treatment. Also wall reflection effects and wall boundary conditions from k equation were enabled under the Reynolds-stress options section. This option enables a transport equation to be solved for the kinetic energy, which is then used to find the boundary conditions of the Reynolds stresses [9].

Next the boundary conditions were set up. All walls were set up as stationary walls with the no slip condition. The wall roughness coefficients were left as default values. For the inlet condition a velocity magnitude of 25 m/s was applied. This resulted in a free stream velocity of 26.4 m/s at the cavity location. The outflow boundary condition was imposed on the tunnel outlet, which required no fields to be specified.

The model was solved with a standard first order upwind discretization scheme using the default under-relaxation constants. In order to decrease computation time the model was solved with a standard k-ε model in order achieve an initial solution before applying the more complex RSM viscous model. The solution was further iterated until all residuals, including the drag coefficient on the cavity walls converged to a value below $10^{-3}$. All numerical results were taken from these converged solutions.

The cavity centre was placed 32D downstream of the tunnel inlet, in order to simulate the fully developed turbulent boundary layer, similar to the one observed in the experiments. The boundary layer parameters for the experimental and simulated data are shown in Table 1.

For the simulated results the values of $u_*/U_o$ and $c_f$ were taken from the data calculated by the software. The other parameters were calculated using an average of 3 vertical profiles located at X = 0 and Z/D = -1, 0 and +1. This was similar to the procedure completed in the experiments. The boundary layer parameters scaled with the cavity diameter resulted in $\delta$/D = 0.74, $\delta_*$/D = 0.09 and $\delta_\theta$/D = 0.07.

| Boundary Layer Parameter | Experimental | CFD | % Difference with regard to exp. data |
|---|---|---|---|
| $\delta$ (mm) | 54.7 ± 5.6 | 61.0 | 11.5 % |
| $\delta_*$ (mm) | 7.0 ± 0.1 | 5.5 | 21.4 % |
| $\delta_\theta$ (mm) | 5.1 ± 0.1 | 3.9 | 23.5 % |
| $c_f$ | 0.0030 ± 0.0002 | 0.0027 | 10.0 % |
| $u_*$ / $U_o$ | 0.042 ± 0.0012 | 0.037 | 11.9 % |

*Table 1: Boundary layer parameters for the experimental and simulated results*

## 5. COMPARISON TO EXPERIMENTAL DATA

The experimental data for the approaching flow boundary layer were first compared to the simulated data. Once this was complete a series of h/D ratios was examined to validate the software's ability to model different cavity flow configurations.

First, using the pressure transducer data collected from the experiment, the pressure coefficient distributions on the cavity walls and the tunnel ground plane near the cavity were examined and compared to the simulated results. The next step involved the comparison of pressure distributions along the cavity centre line for the upstream wall, base and downstream wall. Then, wake profiles collected by the hot wire anemometer were compared to assess the effect of the cavity on the main boundary layer flow. Lastly, the drag coefficient due to the presence of the cavity was compared between the two data sets. These comparisons were completed for all three h/D ratios examined in the experimental procedure.

The pressure distributions on the cavity sidewall were "unwrapped" with theta = 0° corresponding to the upstream cavity edge and theta = 180°

being the downstream cavity edge. For all other profiles the flow direction was from left to right.

Errors associated with the experimental equipment resulted in an uncertainty in the experimental results of ±0.003 Cp based upon a nominal value of 0.15 Cp. This uncertainty is shown in all the plots when examining the centre line profiles.

## 5.1 Boundary Layer Parameters

Only a small discrepancy was found between the resulting boundary layer parameters for the simulations and experimental data. Some of the difference can be attributed to spanwise imperfection in the flow used in the experiments.

## 5.2 Pressure Coefficient Profiles for h/D = 0.7

From the three different configurations simulated the h/D ratio of 0.7 compared the best to the experimental data. Similar patterns of pressure coefficient distributions were observed between the two data sets on the cavity surfaces. The main difference was in the magnitude of the Cp values themselves. In general the simulated results showed Cp values lower than found in the experiment, which is why the contour plots do not match exactly in Figure 5. But, when examining the simulated results under a different scaling, a similar pattern was observed as in the experimental data, as seen in Figure 6. The region of shear layer impingement is also well defined in the simulated results, indicated by the high pressure coefficients seen near the lip of the cavity on the downstream cavity edge in Figure 6, although the experimental reattachment zone is somewhat split while the numerical is unified.

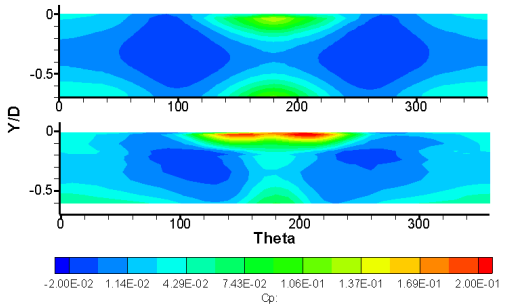


*Figure 5: h/D = 0.7 Cavity side wall, simulated (top), experimental(bottom)*

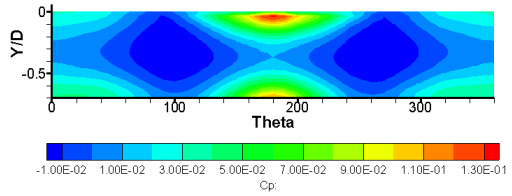


*Figure 6: h/D = 0.7 Simulated Cavity side wall, (with modified Cp contour scaling)*

The general shape and location of the stable vortex found in the cavity was also well defined in the simulated results as seen in Figure 6 and Figure 7. The main difference was the lack of curvature of the vortex tube inside the cavity. The simulated results tend to indicate a straighter vortex tube spanning the cavity, seen on the cavity base in Figure 7. The simulated results showed the large negative pressure region with a smaller curvature than seen in the experimental results. The lack of curvature was also seen on the cavity sides, as the circular regions of low pressure were found at slightly different theta angles than in the experimental results.

The general trend was for the simulated results to underestimate the magnitude of the Cp values on the cavity surfaces but predict similar patterns. Examining the Cp distribution down the centreline of the cavity along the upstream wall, bottom and downstream wall further confirmed this statement, as the software constantly predicted lower Cp values with similar trends in the shape of the distribution.

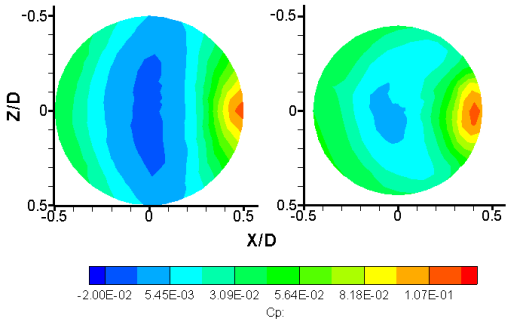


*Figure 7: h/D = 0.7 Cavity base, simulated (left), experimental (right)*

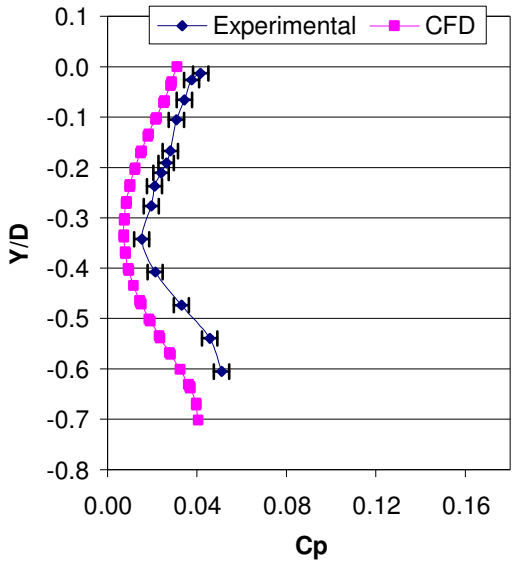


*Figure 8: h/D = 0.7, Upstream cavity wall (0°)*

As seen in figures Figure 8, Figure 9 and Figure 10 the Cp values deviated by as much as 0.02 between the two sets of data. This is similar to a previous study [10], which also found lower Cp values for the simulated profiles, while displaying similar trends as the experimental results along the cavity centreline for rectangular cavities. In that study the Cp values varied by as much as 0.05 compared to the experimental results. The range of uncertainty in the Cp values for the experimental results is also shown in the plots.

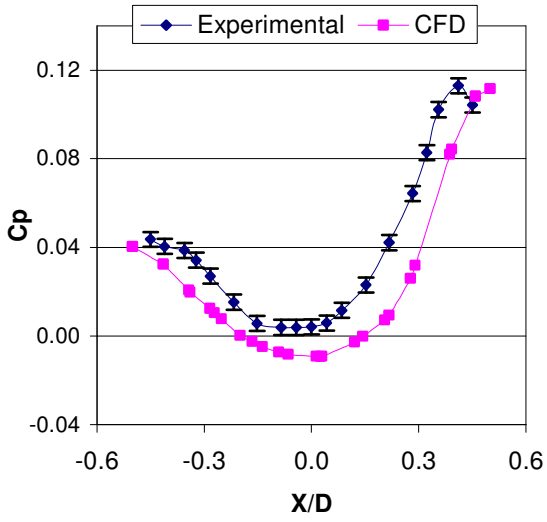


F*igure 9: h/D = 0.7 Cavity base*

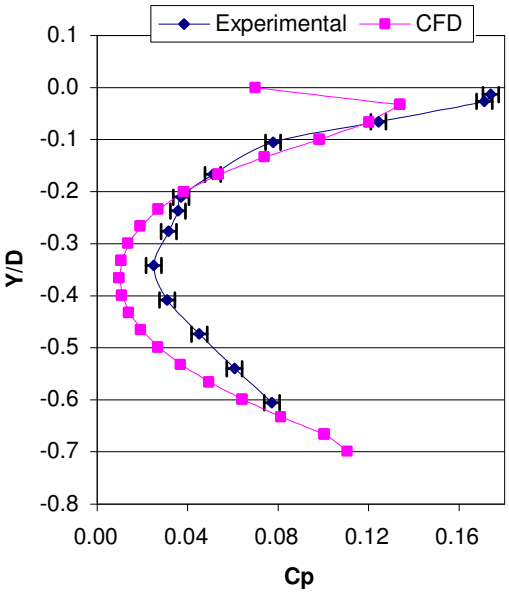


*Figure 10: h/D = 0.7 Downstream cavity wall (180°)*

This h/D = 0.7 configuration was also compared in terms of normalizing the pressure coefficient with the friction velocity. The maximum difference between the experimental and simulated data decreased only by 0.0057 Cp using the friction velocity scaling. This was mainly due to the small variation between the boundary layers, as mentioned previously. The resulting profiles with this decreased difference is shown in Figure 11.

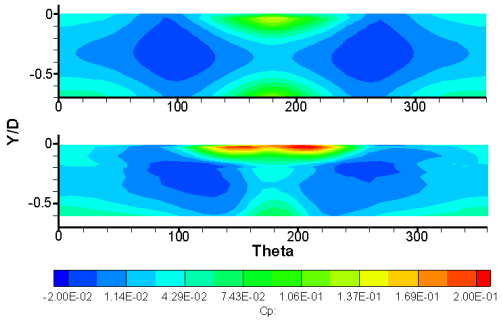


*Figure 11: h/D = 0.7 Cavity side wall, normalized by friction velocity, simulated (top), experimental (bottom)*

There was also reasonable agreement between the data sets when examining the ground plane surrounding the cavity, as seen in Figure 12. A symmetric flow along the downstream axis was predicted by FLUENT, which was also observed in the experiment, as indicated by the symmetric

low pressure regions downstream of the cavity.

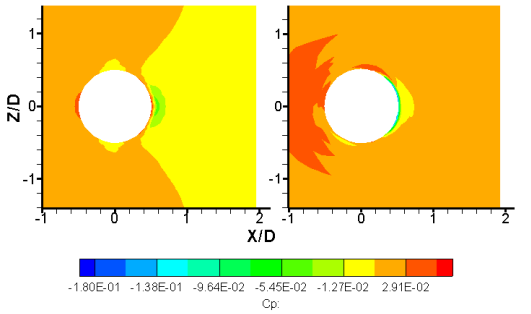


*Figure 12: h/D =0.7 Ground plane around the cavity, simulated (left), experimental (right)*

## 5.3 Pressure Coefficient Profiles for h/D = 0.2

Similar to the h/D = 0.7 configuration, the profiles of Cp distributions on the cavity surfaces and ground plane were in good agreement with the experimental data. A major difference was observed on the downstream edge of the cavity sidewall, near the lip where the shear layer reattachment was not well predicted by FLUENT, seen in Figure 13. This reattachment region was not predicted at all as it did not even appear when the simulated results were examined on a different scale as seen in Figure 14. This is the area where the largest difference in pressures was observed between the two data sets when examining the pressures along the cavity centreline. The downstream wall had a maximum difference of 0.08 in Cp, while the other plots deviated from the experimental results by less than 0.03.

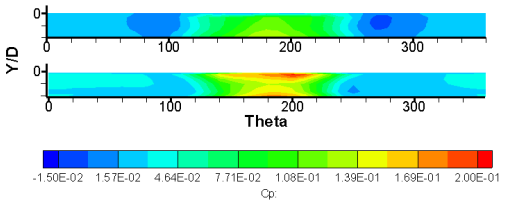


*Figure 13: h/D = 0.2 Cavity side wall, simulated (top), experimental (bottom)*

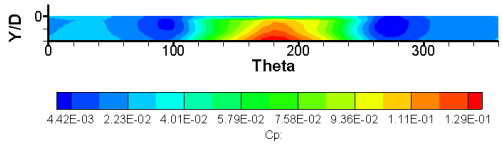


*Figure 14: h/D = 0.2 Simulated cavity side wall (with modified Cp contour scaling)*

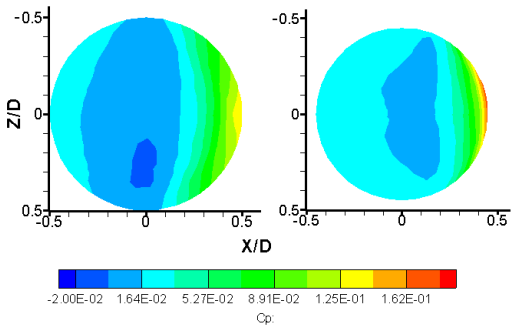


*Figure 15: h/D = 0.2 Cavity bottom, simulated (left), experimental (right)*

Examining the cavity base in the experimental data, it appears that the flow is still an open type, due to a large negative pressure region similar to that found in the h/D = 0.7 case. This was also indicated by the simulated results, as seen in Figure 15. The dominant vortex is not clearly shown in the experimental cavity sidewall pressures, most likely due to limited number of pressure taps along the sidewall. However the large negative pressure region on the cavity base shows the likelihood of a vortex structure in the cavity volume. A symmetric flow was also seen in the pressure coefficient distributions along the ground plane, Figure 16 near the cavity for both the experimental and simulated data.

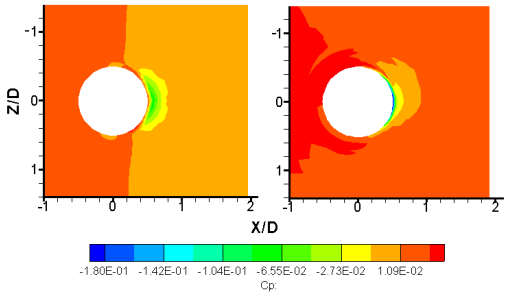


*Figure 16: h/D = 0.2 Ground plane around the cavity, simulated (left), experimental (right)*

## 5.4 Pressure Coefficient Profiles for h/D = 0.47

Asymmetric flow was seen in the simulated results for this configuration as also observed in the experimental data. The angle made with the free stream direction by the main vortex was

used as the measure of strength of the asymmetry, keeping in mind that a symmetric flow would result in an angle of 90˚. FLUENT indicated an angle of about 60˚ while that found in the experiment was approximately 45˚, as seen in Figure 18.

The sense of the asymmetry could not be compared as the asymmetry is marginally stable and could be switched in the experiment. Therefore, a same sense experimental data set was chosen for the comparison.

The asymmetry was also seen in the cavity sidewall plots, Figure 17. It is interesting to note that the vortex centres were predicted by the software at approximately the same angles as for the experiment, even thought the cavity base plots did not agree in the same manner. This is similar to the h/D = 0.7 case where the vortex centres were predicted with more accuracy on the cavity side wall than on the cavity base, as indicated by regions of low pressure.

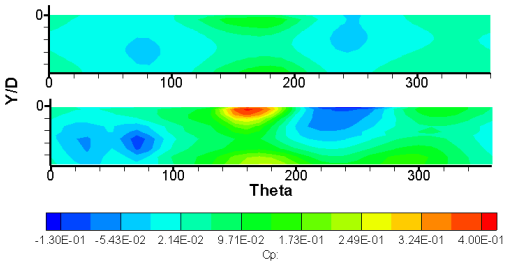


*Figure 17: h/D = 0.47 Cavity side wall, simulated (top), experimental (bottom)*

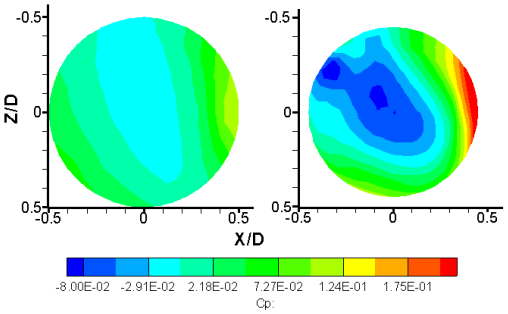


*Figure 18: h/D = 0.47 Cavity base, simulated (left), experimental (right)*

In addition to the software being unable to predict the corresponding angle of the vortex tube with respect to the free stream direction, FLUENT also did not show a clear representation of the raised vortex issuing out of the cavity. As seen in Figure 19, the vortex centre near 240˚ is not as close to the cavity lip as seen in the experiments. This indicates that only a small portion of the vortex tube penetrating into the boundary layer for the simulated results, compared to the experimental data, where a larger portion of the vortex entered into the main stream flow. The lack of low Cp regions on the ground plane in Figure 20 reveals that the trailing vortex is not evident in the simulated results as compared to the experimental data.

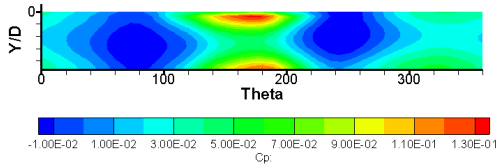


*Figure 19: h/D = 0.47 Simulated cavity side wall, (with modified Cp contour scaling)*

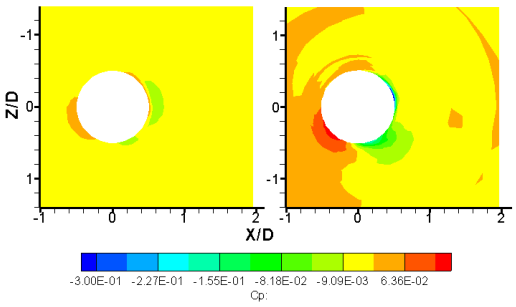


*Figure 20: h/D =0.47 Ground plane around the cavity, simulated (left), experimental (right)*

Due to the resulting asymmetric flow for h/D = 0.47 only the downstream cavity edge (180˚) resembled the trend seen in the experimental data. The difference between the simulated and experimental data for the downstream wall was much greater than for the other two configurations. The maximum difference for this edge was 0.2 in Cp, as seen in Figure 21, as compared to 0.02 and 0.03 Cp for h/D = 0.7 and h/D =0.2 configurations, respectively.

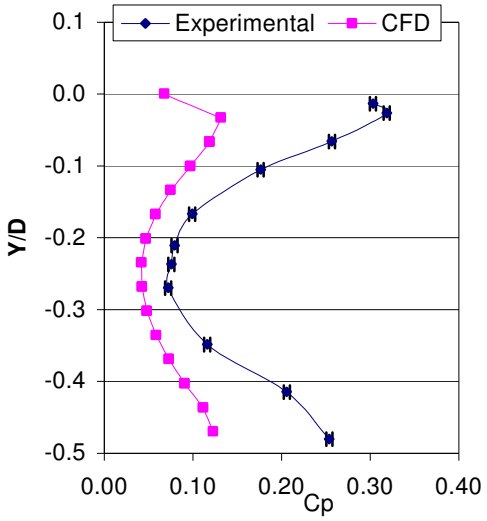


*Figure 21: h/D = 0.47 Downstream cavity wall (180°)*

## 5.5 Resulting Velocity Defect in the Wake

Using the hot wire anemometer data the velocity defect in the wake could be examined. The velocity field with the no cavity case was subtracted from the velocity field with the cavity in place. This result was then divided by the free stream velocity. The profiles for h/D = 0.2 and 0.47 are plotted in Figure 22 and Figure 23, respectively. The uncertainty in the hot wire measurements was 0.4m/s.

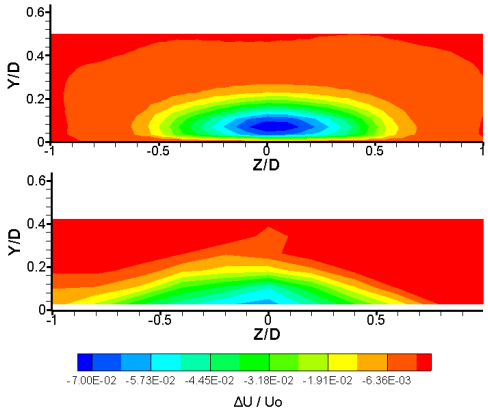


*Figure 22: h/D =0.2, Velocity defect in wake, simulated (top), experimental (bottom)*

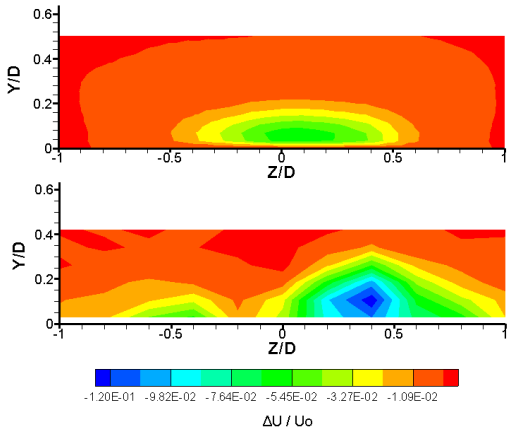


*Figure 23: h/D =0.47, Velocity defect in wake, simulated (top), experimental (bottom)*

Due to limitations in the experimental equipment the hot wire data do not completely reach the ground plane (Y/D = 0).

For h/D = 0.2, the symmetric resulting flow is apparent by the largest velocity defect being centred at the mid-point of the cavity. However, the spanwise length of the velocity defect is much smaller for the simulated case than for the experimental data.

The asymmetric flow for h/D = 0.47 is shown in Figure 23 although, as previously mentioned, the asymmetry is not as strong as observed in the experiments. The weaker asymmetry resulted in the maximum velocity defect being more centred than seen in the experimental results.

As previously mentioned, the dominant vortex tube did not penetrate into the main stream flow as much as in the experiment, therefore less disturbance was introduced into the boundary layer flow above the cavity. This resulted in the larger difference in the magnitudes of the velocity defect between the experiments and the CFD as compared to the h/D = 0.2 case.

## 5.6 Drag Coefficient increase due to the Cavity

The resulting drag coefficient on the cavity sidewall was calculated for both the experimental and simulated data. The skin friction coefficient was then subtracted from this value to obtain the net drag coefficient due to the cavity. For the experimental data, the pressure measurements were integrated along the cavity sidewall. The error in the net drag coefficient was estimated to be ± 0.0037.

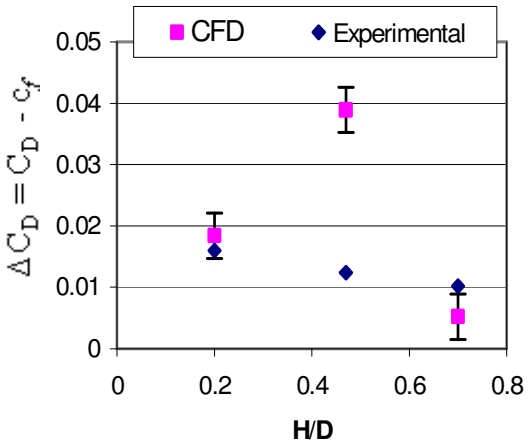


*Figure 24: Drag coefficient increase due to the cavity*

As seen in Figure 24, the net drag coefficient for the simulated results only deviates dramatically at the h/D = 0.47 ratio. This is due to the lack of a trailing vortex in the simulated results. This trailing vortex sweeps higher momentum fluid into the cavity and causes an increase in drag, as observed in the experimental results.

## 6. Conclusions and Future Work

The simulated results show a good representation of the flow physics involved in cavity flows at most of the h/D configurations tested. The main difference was in the under estimation of the Cp values along all the surfaces. The patterns of vortex centres and shear layer reattachment was indicated quite well for the h/D = 0.7 case. The difference in Cp values along the cavity centreline was also the smallest compared to the other two configurations tested.

The shear layer reattachment region near the lip was not predicted at all for h/D = 0.2, which is contradictory to experimental results. However, the dominant vortex tube and velocity defect closely resembled the experimental data for this configuration.

The largest discrepancy between simulated and experimental data was for h/D = 0.47 case. Although asymmetric flow was predicted by FLUENT, which is a very distinct feature of the resulting flow for this h/D ratio, the strength of the asymmetry was weaker than observed in the experiment. This had a great influence on the velocity defect and the Cp distributions along the cavity surfaces.

The net drag coefficient due to the cavity seemed to be well predicted by the simulated results except for the h/D = 0.47 case. The large discrepancy at this configuration is due to the weaker asymmetry seen in the flow.

Future work will encompass the application of different turbulence models to the simulations to check whether they can predict cavity flows with a greater accuracy then the model currently used. Future work will also include the modeling of the problem in an unsteady solution to compare to the experimental data for pressure and velocity fluctuations.

## 7. Acknowledgments

The current work was funded by the Natural Sciences and Engineering Research Council of Canada (NSERC).

## 8. Nomenclature

| | |
|---|---|
| Cp | Pressure coefficient |
| $C_D$ | Drag coefficient |
| D | Cavity diameter |
| h | Cavity depth |
| P | Pressure measurement |
| $P_s$ | Static pressure |
| $U_o$ | Reference velocity |
| ρ | Density |
| $\delta$ | Boundary layer thickness |
| $\delta_*$ | Displacement thickness |
| $\delta_\theta$ | Momentum thickness |
| $\tau_w$ | Shear stress near the wall |
| $c_f$ | Skin friction coefficient |
| $u_*$ | Friction velocity |

## 9. References

[1] Roshko A., “Some measurement of flow in a rectangular cutout”, NACA TN 3488, 1955.

[2] Pozrikidis C., "Shear flow over a plane wall with an axisymmetric cavity or a circular orifice of finite thickness", Master’s Thesis, University of California at San Diego, 1993.

[3] Friesing H., “Measurement of the drag associated with recessed surfaces: cut-outs of rectangular and elliptical planform”, Z.W.B.F.B 628 (R.A.E Library Translation 1614), 1971

[4] Hiwada M., Kawamura T., Mabuchi I., Kumada M., “Some Characteristics of Flow Pattern and Heat Transfer past a Circular Cylindrical Cavity”, Bulletin of the JSME, **26** (220): 1744-1752, 1983.

[5] Savory E., Toy N., Gaudet L., “Effect of lip configuration on the drag of a circular cavity”, Emerging Techniques in Drag Reduction, Mechanical Engineering Publications Ltd, pg.317-335, 1996.

[6] Gaudet L., Winter K.G., “Measurements of the drag of some characteristic aircraft excrescences immersed in turbulent boundary layers”, R.A.E. Technical Memorandum Aero., 1973

[7] Dybenko J., “An experimental investigation of turbulent boundary layer flow over surface-mounted circular cavities”, Master’s Thesis, University of Western Ontario, 2005.

[8] Dubief Y., Delcayre F., “On coherent-vortex identification in turbulence”, Journal of Turbulence, **1**, Article 011, 2000.

[9] Fluent 6.0 Documentation, Fluent User’s Guide, 2001

[10] Czech M., “The acoustics and aerodynamics of turbulent flow over yawed rectangular cavities”, PHD Thesis, University of Surrey, 2000.